


Control of the excited-to-ionized atoms ratio in a dense gas in the wake of an intense femtosecond laser pulse

Suyash Bajpai ¹ and Dmitri A. Romanov ^{1,2}

¹*Department of Physics, Temple University, Philadelphia, Pennsylvania 19122, USA*

²*Center for Advanced Photonics Research, College of Science and Technology, Temple University, Philadelphia, Pennsylvania 19122, USA*

 (Received 28 December 2021; accepted 7 April 2022; published 28 April 2022)

We demonstrate the sensitivity of the plasma composition in the filament wake channel in a dense gas to the temporal shape of the driving femtosecond laser pulse. During the pulse, the electrons released via strong-field ionization and driven by oscillating laser field are actively engaged in collisional processes with neutral neighbor atoms, including inverse Bremsstrahlung, impact ionization, and collisional excitation. By the end of the pulse, these collisional processes produce considerable numbers of additional free electrons (or ionized atoms) and excited atoms, and these contents of the filament wake channel determine its subsequent evolution dynamics. Addressing the case of high-pressure argon gas and using a kinetic model of these competing collisional processes, we explore the sensitivity of the resulting excited-to-ionized atoms number density ratio to the envelope shape of the driving laser pulse. By considering several families of pulses, we show that asymmetric pulse envelopes skewed toward the earlier time allow for efficient control of the ratio of excited atoms to ionized atoms. The pulse-shape control of the plasma composition in the immediate wake of the laser pulse projects into control of the wake channel evolution and of the associated transient electronic and optical nonlinearities.

DOI: [10.1103/PhysRevE.105.045210](https://doi.org/10.1103/PhysRevE.105.045210)

I. INTRODUCTION

The laser filamentation process in gases and its consequences have been attracting ever growing attention over the two recent decades [1–3]. One significant consequence is the generation of a filament wake channel, which emerges as a highly nonequilibrium and optically underdense plasma column, typically 10–100 μm in diameter and 10–100 cm in length. In the wake of the laser pulse, this system of energetic free electrons, ions, and remaining neutral atoms (or molecules) evolves toward equilibrium, giving rise to a number of transient effects, which have both fundamental and practical importance and which concern both electronic [4–6] and nuclear degrees of freedom [7–9]. The entire evolution cycle extends to microseconds and even milliseconds, and with the laser repetition rate in the kilohertz range, this may result in an altered quasisteady state of the gas medium [10,11]. This panoply of shorter- and longer-term effects in the filament wake channel is predicated and preconditioned by the state of the plasma contents at the end of the laser pulse.

The postpulse electronic dynamics in atmospheric-pressure gases have been extensively investigated experimentally using transverse interferometry [12,13], four-wave mixing [4,5,14], and Rabi sideband emission [15,16]. The results of these measurements agree well with the results of numerical simulations based on thermalized electron gas dynamics assisted by impact ionization cooling [4,5,17].

The strong-field electronic dynamics becomes drastically different in the dense-gas situation, in which the free electrons released in the strong-field ionization and driven by

the oscillating laser field collide intensely with the neighboring neutral atoms. The dense-gas criterion is conveniently expressed in terms of the ponderomotive radius, that is, the length of the electron excursions in the oscillating field, $a_p = (eE_0)/(m\omega^2)$, where E_0 is the laser electric field amplitude and ω is the carrier frequency. A gas of a given number density n_0 is considered dense once $n_0(a_p)^3 \sim 1$: this situation can be effected by high gas pressure, or longer carrier wavelength, or, to a lesser extent, higher laser intensity.

There are three major differences in the ways the intense laser pulse interacts with a tenuous gas and with a dense gas. First, in tenuous gases, the constituent atoms or molecules are only ionized by the immediate action of the strong, non-resonant laser field, with the ionization mechanism varying between the limiting cases of multiphoton ionization and Ammosov-Delone-Krainov (ADK) ionization, depending on the situation [18,19]. In contrast, in a dense gas, the impact ionization by accelerated free electrons plays a considerable role. Second, in tenuous gases, the released electrons gain energy via acceleration by the laser field and scattering off their parent ions. In contrast, in a dense gas, the electrons gain energy mainly via inverse Bremsstrahlung on neutral atoms. Third, in tenuous gases, the strong-field ionization concerns individual atoms or molecules, and so in nonresonant cases, the production of excited atoms is negligibly small. In contrast, in a dense gas, a considerable number of neutral atoms can become excited via collisional excitation. This massive presence of excited atoms after the laser pulse leads to considerable modification in the wake channel evolution, primarily by engaging the Penning ionization mechanism [6,20].

The character of the plasma channel evolution in a dense gas in the laser pulse wake is thus largely determined by the density ratio of excited and ionized atoms at the end of the pulse. The electronic stage of this after-pulse evolution, which proceeds on a picosecond timescale, is described by the set of diffusion-reaction equations for the electron, ion, and excited atom densities, the electron temperature, and the induced electric field [20]. This evolution of the electronic degrees of freedom is reflected in transient linear and nonlinear optical characteristics of the wake channel that can be accessed by probe laser pulses. Moreover, as the electronic system evolution initiates and feeds into the aforementioned longer-term gas-dynamics processes in the channel, these latter processes can also be affected and controlled by relative changes in the concentrations of excited and ionized atoms in the immediate pulse wake.

In this paper, we investigate the possibilities of controlling the emerging plasma buildup in a dense gas subjected to an intense, ultrashort laser pulse. We use the kinetic model [21] for the concerted evolution of the field-driven free electrons, the ions emerging from impact ionization, and the neutral atoms undergoing collisional excitation. As will be seen, the effective control of the wake channel plasma contents is made possible by the competition among collisional processes during the laser pulse. To anchor our description in a specific material system that has been investigated experimentally, we consider an argon gas at an elevated pressure of 60 atm, interacting with an 800-nm laser pulse, which has focal intensity of about 10^{14} W/cm² [6]. To reveal and elucidate the effects of the laser pulse shape, we consider several families of pulses that differ from one another by the shape of their envelope functions but are normalized either by the pulse fluence or by the cumulative strong-field ionization output.

II. MODEL

During the laser pulse, the free electrons emerge initially from the strong-field ionization of the constituent atoms, and they become immediately engaged in the three major field-driven impact processes: (i) energy gain via inverse Bremsstrahlung; (ii) impact ionization, which is associated with both the energy loss by the free electrons and the generation of new free electrons; (iii) collisional excitation of neutral atoms, which is also associated with energy loss by the free electrons. These processes compete among themselves, and this competition allows for their cumulative outcome at the end of the laser pulse to be controlled by the pulse shape.

We consider a high-pressure argon gas subjected to a strong, linearly polarized laser field, $\mathbf{E}(t) = \hat{\mathbf{e}}E_0s(t)\cos(\omega t)$, where $\hat{\mathbf{e}}$ is the polarization vector, E_0 is the laser electric field amplitude, ω is the carrier frequency, and $s(t)$ is a normalized dimensionless envelope function; and we use the kinetic model outlined in Refs. [20,21].

As the free electrons continue emerging during the laser pulse, their laser-driven kinetics is convenient to describe using not the distribution function but the local density of occupied energy states, $n(\varepsilon, t)$, so that the total electron number density is $n_e(t) = \int_0^\infty d\varepsilon n(\varepsilon, t)$, and the average electron energy is $\bar{\varepsilon}(t) = (\int_0^\infty d\varepsilon \varepsilon n(\varepsilon, t))/n_e(t)$. The evolution of $n(\varepsilon, t)$ is determined by the strong-field ionization and the mentioned

impact processes during the laser pulse:

$$\frac{\partial n}{\partial t} = \frac{\partial n}{\partial t}\Big|_{s-f} + \frac{\partial n}{\partial t}\Big|_B + \frac{\partial n}{\partial t}\Big|_{\text{ion}} + \frac{\partial n}{\partial t}\Big|_{\text{ex}}. \quad (1)$$

In this equation, the first term in the right-hand side is the source term, which describes the generation of free electrons through the atomic strong-field ionization, with the ionization rate $W(t)$. For argon atoms and the laser intensities of our interest, $\sim 10^{14}$ W/cm², the value of the Keldysh parameter γ is about 1.15; it was shown that at these values of γ it is still possible to use the ADK formula [22] as a good approximation for the ionization rate [18,19] at this borderline between the tunneling and the multiphoton regimes:

$$W(t) = \left(\frac{6}{\pi}\right)^{1/2} \frac{2^{2n^*+3}}{(n^*)^3 \Gamma(2n^*)} \left(\frac{Ry}{\hbar}\right) \left(\frac{4E_a}{E_0s(t)(n^*)^3}\right)^{2n^*-3/4} \times \exp\left(-\frac{4E_a}{E_0s(t)(n^*)^3}\right), \quad (2)$$

where $E_a = Ry/(ea_B) \approx 51.42$ V/Å is the atomic unit of electric field and $n^* = \sqrt{Ry/(2\varepsilon_{\text{ion}})}$, with $\varepsilon_{\text{ion}} = 15.76$ eV being the ionization energy. The use of the ADK approximation becomes even more justified as we consider shorter pulses with higher peak intensities (e.g., $\gamma = 0.96$ at the laser intensity of 1.4×10^{14} W/cm²). In what follows, we only consider situations with low cumulative degree of strong-field ionization, and this means that (i) we can safely assume that the ionization occurs mainly near the peak of the pulse and disregard possible change of the ionization mechanism in the pulse wings; (ii) any effects of the ground-state population depletion during the pulse can be neglected. (It should be noted, however, that the conceptual conclusions and qualitative results of what follows are not tied to a specific mechanism of strong-field ionization, because a much greater part of the eventual ionization will be caused by the impact processes, with the direct strong-field ionization by the laser field merely providing the seed electrons.) Then, the source term is written as $(\partial n/\partial t)|_{s-f} = g(\varepsilon)n_0W(t)$, where n_0 is the density of neutral atoms and $g(\varepsilon)$ is an auxiliary function, which accounts for the initial energy distribution of the emerging, field-driven electrons upon first elastic scattering. (The electrons emerge with low kinetic energy, but upon the first cycle of laser-field acceleration and elastic scattering, which is beyond our model framework, they acquire some initial energy distribution.) The specific form of this seed function is of no particular importance; we choose $g(\varepsilon) = C_{m\mu}\varepsilon^m\{1 - \tanh[\mu(\varepsilon - U_p)]\}$, where m and μ are adjustable parameters, $C_{m\mu}$ is the normalization constant, and $U_p = (eE_0)^2/(4m\omega^2)$ is the ponderomotive energy.

The second term on the right-hand side of Eq. (1) represents the transformation of the energy distribution function due to the inverse Bremsstrahlung on neutral atoms. Assuming the laser carrier frequency to be greater than the elastic scattering rate of an electron on neutral atoms, which in turn is greater than the inverse of the shortest characteristic timescale in the pulse envelope, this term is obtained [21] as

$$\frac{\partial n}{\partial t}\Big|_B = \frac{4}{3}\sqrt{\frac{2}{m}}n_0\sigma_{\text{tr}}(\varepsilon)U_p s^2(t)\frac{\partial}{\partial \varepsilon}\left[\sqrt{\varepsilon}\left(\varepsilon\frac{\partial n}{\partial \varepsilon} - \frac{1}{2}n\right)\right]. \quad (3)$$

Here, $\sigma_{\text{tr}}(\varepsilon)$ is the cross section for elastic scattering, which can be considered virtually constant, $\sigma_{\text{tr}}(\varepsilon) \approx \sigma_0 = 10^{-15} \text{ cm}^2$, as the relevant energy range (5–20 eV) lies well away from the Ramsauer minimum [23]. This Fokker-Planck-type term describes the effective electron-density diffusion along the energy axis, with the time-dependent diffusion coefficient [24].

The third term on the right-hand side of Eq. (1) expresses the effects of impact ionization of neutral atoms by the energetic free electrons; it reads

$$\begin{aligned} \left. \frac{\partial n}{\partial t} \right|_{\text{ion}} &= -v_{\text{ion}}(\varepsilon)n(\varepsilon, t)\Theta(\varepsilon - \varepsilon_{\text{ion}}) \\ &+ v_{\text{ion}}(\varepsilon + \varepsilon_{\text{ion}})n(\varepsilon + \varepsilon_{\text{ion}}, t) \\ &+ g(\varepsilon) \int_{\varepsilon_{\text{ion}}}^{\infty} d\varepsilon' v_{\text{ion}}(\varepsilon')n(\varepsilon', t), \end{aligned} \quad (4)$$

where $\varepsilon_{\text{ion}} = 15.76 \text{ eV}$ is the ionization energy. (As the resulting degree of ionization in actual cases is on the order of 10^{-2} , we neglect the depletion of the neutral-atom population.) In this expression, the first two contributions correspond to the general downshift of the electron energy distribution due to kinetic energy expenditure on the ionization. That is, the number of electrons at a given energy ε is decreasing as some electrons move to the energy position of $\varepsilon - \varepsilon_{\text{ion}}$ due to the impact ionization of neutral atoms; at the same time, new electrons arrive at ε as they are being in turn shifted down from $\varepsilon + \varepsilon_{\text{ion}}$. The third contribution accounts for the new electrons that emerge from this ionization and join the field-driven collective.

For the impact ionization rate, $v_{\text{ion}}(\varepsilon)$, we use the semiempirical Lötzt formula for the total ionization cross section [25]. In this formula, the cross section is given by the sum of subshell contributions; for Ar and for the electron energies in question, it is sufficient to consider only the contribution of the eight electrons of the uppermost shell. Then, $v_{\text{ion}}(\varepsilon)$ is obtained as

$$\begin{aligned} v_{\text{ion}}(\varepsilon) &= 3.63\nu_0 \sqrt{\frac{\varepsilon_{\text{ion}}}{\varepsilon}} \left[1 - 0.62 \exp\left(-0.40 \frac{\varepsilon - \varepsilon_{\text{ion}}}{\varepsilon_{\text{ion}}}\right) \right] \\ &\times \ln\left(\frac{\varepsilon}{\varepsilon_{\text{ion}}}\right) \Theta(\varepsilon - \varepsilon_{\text{ion}}), \end{aligned} \quad (5)$$

where $\varepsilon_{\text{ion}} = 15.76 \text{ eV}$ is the ionization energy and $\nu_0 = 1.35n_0\pi a_B^2 (Ry/\varepsilon_{\text{ion}})^2 \sqrt{2\varepsilon_{\text{ion}}/m}$. As a function of energy, $v_{\text{ion}}(\varepsilon)$ has a threshold at ε_{ion} , and then it rises sharply throughout the range of energies pertinent to the $n(\varepsilon, t)$ evolution.

The fourth term in the right-hand side of Eq. (1) describes the effects of collisional excitation of neutral atoms. In a way similar to impact ionization, in the act of collisional excitation, an energetic electron collides with a neutral atom and promotes the latter to an excited state with the excitation energy, ε_{ex} , at the expense of the kinetic energy loss. As a result, the free electrons are reshuffled along the energy axis via finite energy shifts, so that

$$\left. \frac{\partial n}{\partial t} \right|_{\text{ex}} = -v_{\text{ex}}(\varepsilon)n(\varepsilon, t)\Theta(\varepsilon - \varepsilon_{\text{ex}}) + v_{\text{ex}}(\varepsilon + \varepsilon_{\text{ex}})n(\varepsilon + \varepsilon_{\text{ex}}, t). \quad (6)$$

The concomitant growth of the total number of the excited atoms is determined by the expression

$$\frac{dn_{\text{ex}}}{dt} = \int_{\varepsilon_{\text{ex}}}^{\infty} d\varepsilon v_{\text{ex}}(\varepsilon)n(\varepsilon, t). \quad (7)$$

Using the semiempirical formula of Ref. [26] for the cumulative excitation cross section, the effective excitation rate is obtained as

$$v_{\text{ex}}(\varepsilon) = \nu_0 \left(\frac{\varepsilon_{\text{ion}}}{\varepsilon_{\text{ex}}}\right)^{3/2} \left(\frac{\varepsilon_{\text{ex}}}{\varepsilon}\right)^{0.25} \left(1 - \frac{\varepsilon_{\text{ex}}}{\varepsilon}\right)^2 \Theta(\varepsilon - \varepsilon_{\text{ex}}), \quad (8)$$

As a function of energy, $v_{\text{ex}}(\varepsilon)$ has a threshold at $\varepsilon = \varepsilon_{\text{ex}}$, and near this threshold it rises according to a power law.

When considering the process of collisional excitation, strictly speaking, there are several accessible excited atomic states, so that the right-hand side in Eq. (6) should have contributions from transitions related to all of these states with the respective excitation rates. However, we will restrict our model with one representative excited state, which has the excitation energy of $\varepsilon_{\text{ex}} = 11.8 \text{ eV}$.

The character and outcomes of the competition of the impact ionization and collisional excitation processes are determined by the energy-dependent rates of these processes, $v_{\text{ion}}(\varepsilon)$ and $v_{\text{ex}}(\varepsilon)$. Since $v_{\text{ex}}(\varepsilon)$ has its inception point at a smaller value of energy than that for $v_{\text{ion}}(\varepsilon)$, there is an energy interval in which $v_{\text{ex}}(\varepsilon) > v_{\text{ion}}(\varepsilon)$. When the field-driven electrons climb up the energy axis, they inevitably enter this region, and thus impact ionization is necessarily accompanied by collisional excitation. The relative outcome of these two processes is determined by the details of the field-driven electron dynamics during the pulse, and may well be modified by changes in the pulse shape.

It should be noted that in the foregoing discussion we did not consider processes of impact ionization of the excited atoms. It can be argued that for an individual atom this process is much more likely than the ionization from the ground state. However, if there were no excited atoms at the start of the laser pulse, their concentration remains very low during the most part of the pulse and rises to a few percent only near the end of the pulse [21]. This is so because the free electrons released by the strong-field ionization need first to gain sufficient energy to become engaged in the inelastic collisions producing excited atoms. At the typical values of the resulting excited-atom densities and the free electron densities, the impact ionization of the excited atoms becomes significant only at a longer timescale (about 5 ps) in the after-pulse evolution of the plasma channel [20]. The situation would be different in the case of a sufficient pre-existing concentration of the excited atoms. To avoid possible complications, we presume that the gas is initially at a sufficiently low temperature (e.g., room temperature), so that the initial concentrations of excited and ionized atoms are vanishingly small.

III. RATIO CONTROL

Given the mentioned competition among collisional processes, we explore the possibilities to control the resulting plasma composition by the shape of the laser pulse. Specifically, we concentrate on controlling the ratio of the

final excited-atom and ionic (electronic) densities. As was mentioned in the Introduction, this ratio largely determines the character of the excited medium evolution in the wake of the pulse [6,20]. To investigate the possibilities and limits of the ratio control, we considered three representative families of envelope functions $s(t)$. We have implemented these pulse shapes to solve numerically Eq. (1) with the right-hand side determined by the expressions of Eqs. (3), (4), and (6). From the mathematical standpoint, this is a rather complicated equation, including partial derivatives, integral terms, and finite-difference terms. As such, it is not amenable to standard numerical solvers and requires a tailored approach. The results obtained show that the dynamics of the laser-driven emerging plasma does depend substantially on the pulse shape.

First, we consider the effects of pulse stretch, which in experimental situations can be effected, e.g., by a quadratic spectral chirp [27]. In these spectral phase manipulations, the pulse fluence F is preserved, and so the resulting temporal pulse stretch is accompanied by the decrease in the peak intensity. Accordingly, we consider a family of pulses, in which the fluence is kept constant, while the pulse duration and the peak intensity change in concert. Then, it is convenient to express the laser electric field in the form $\mathbf{E}(t) = \hat{\mathbf{e}}\sqrt{2F/(c\epsilon_0\tau_0)}s_\tau(t)\cos(\omega t)$, where τ_0 is the initially set value of the pulse duration. Upon the stretch, the pulse duration τ and the peak intensity, $I = F/\tau$, change simultaneously, so that the envelope function, $s_\tau(t)$, is normalized as

$$\int_{-\infty}^{\infty} dt s_\tau^2(t) = \tau_0. \quad (9)$$

Specifically, we chose

$$s_\tau(t) = \sqrt{\frac{8\tau_0}{3\tau}} \sin^2\left(\pi \frac{t}{\tau}\right) \Theta(t)\Theta(\tau - t), \quad (10)$$

where $\Theta(t)$ is the Heaviside step function. We used this envelope function in numerical simulations based on Eqs. (1)–(7); the resulting ratios of the excited-atom density to ionized-atom density, depending on the pulse duration and the nominal peak intensity, are presented in Fig. 1 for two different values of the gas pressure: 60 and 40 atm. These ratios reflect the complex interplay of the pulse duration and the peak intensity effects in the evolution of the emerging nonequilibrium plasma, with the results markedly dependent on the gas density. In Fig. 1(a) (at the lower pressure), the $n_{\text{ex}}/n_{\text{ion}}$ ratio depends monotonically on the pulse duration, being greater for shorter and more intense pulses. A similar monotonic behavior is seen in Fig. 1(b) for low values of the pulse energy. However, at higher values of the pulse energy, the dependence of the ratio on the pulse duration develops a well-pronounced maximum. This may reflect the fact that for the collisional processes to take effect, the emerging electron gas needs to be exposed to a relatively intense laser field over a relatively long time. There is a tradeoff, however, as the pulse stretch reduces the peak intensity, thus reducing the strong-field ionization rate and the number of free electrons initiating those very collisional processes. The broad shape of the curves in Fig. 1 is a visible manifestation of this tradeoff.

This consideration leads to a suggestion that the manipulation of the collisional processes will be more pronounced

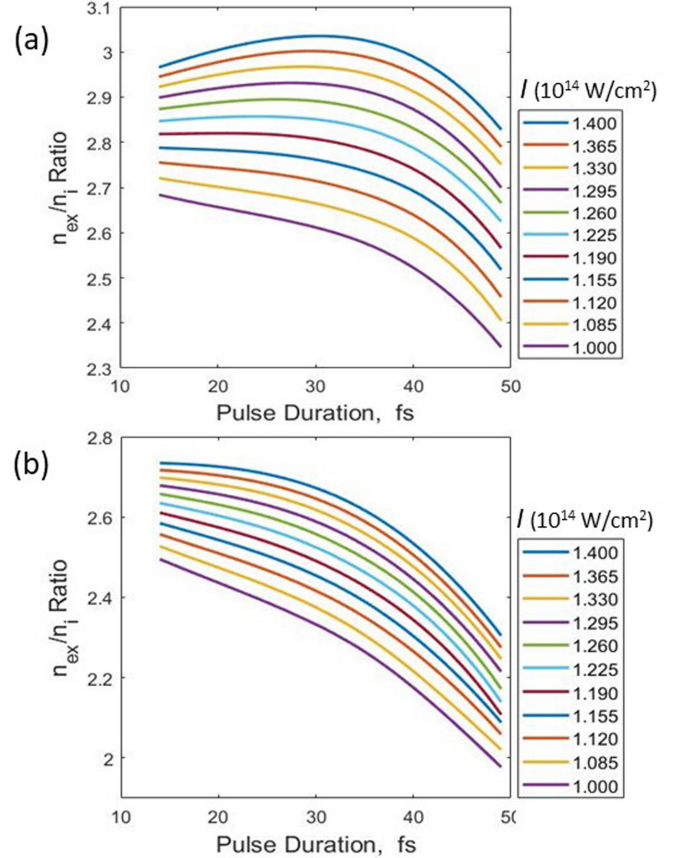


FIG. 1. The effect of the laser pulse stretching on the density ratio of excited to ionized atoms in the immediate pulse wake in a dense argon gas: (a) the gas pressure of 60 atm; (b) the gas pressure of 40 atm. The laser pulse fluence is kept constant; the reference intensity is shown for the FWHM pulse duration of 24 fs.

when using asymmetric pulse shapes. Such pulse shapes can be generated in experiment using, e.g., a combination of quadratic and cubic spectral chirp, that is, with the spectral form $E(\omega) \sim \exp(-\omega^2/(2\sigma) + i\alpha\omega^2 + i\beta\omega^3)$. In this expression, positive values of the parameter β correspond to pulses with the tail extended toward earlier time, whereas negative values of β correspond to the pulses with the tail extended toward later time, see Fig. 2(a). Manipulation of quadratic and cubic spectral chirps are routinely used in pulse compression, where positive cubic chirp is induced, e.g., by an optical fiber and the negative cubic chirp is provided by a dispersive delay line using a combination of prisms or diffraction gratings [28,29]. More versatile controllable spectral chirp manipulation is achieved using phase masks in spatial light modulators [27,30]. For the sake of numerical convenience, we model these skewed pulse envelopes with a one-parameter family of functions determined as

$$s_{a,\tau}(t) = \frac{c(a)}{4} \sqrt{\frac{\tau_0}{\tau}} \left[1 + \tanh\left(\left(1-a\right)\frac{t}{\tau}\right) \right] \left[1 - \tanh\left(a\frac{t}{\tau}\right) \right]. \quad (11)$$

Here, $c(a)$ is the normalization constant, which ensures that the condition expressed by Eq. (9) is satisfied: $c(a) = (2a)^{1/2} (\int_0^\infty dz z(z+1)^{-2} (z^{1/a}-1)^{-2})^{-1/2}$. The shape parameter a varies in the interval $(0, 1)$ and determines the

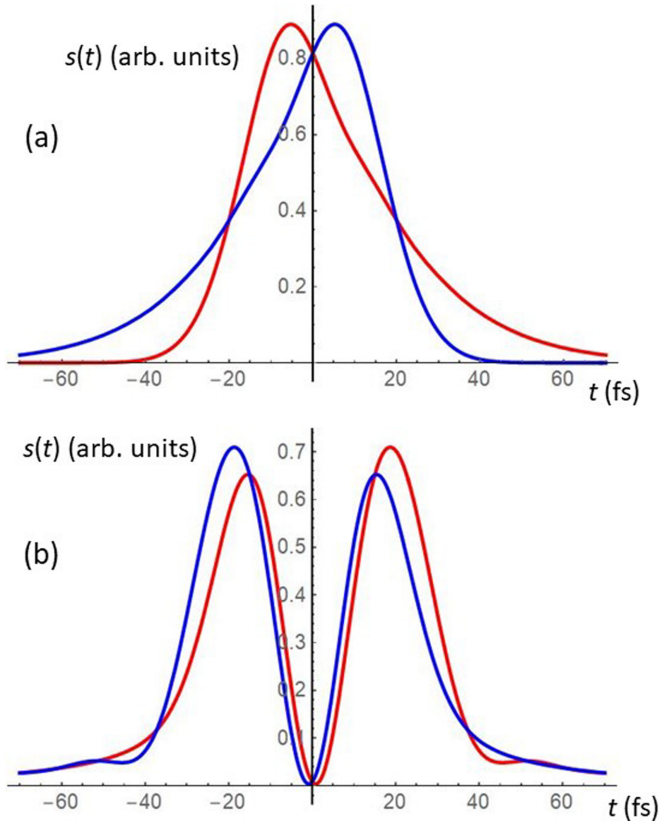


FIG. 2. (a) Asymmetric laser pulses effected by a combination of quadratic and cubic spectral chirp. Red line: positive value of the cubic chirp parameter; blue line: negative value of the cubic chirp parameter. The skewed envelope shapes are modeled by a one-parameter expression of Eq. (10). (b) Double-pulse shapes effected by a π -step phase mask. Red line: positive value of the cubic chirp parameter; blue line: negative value of the cubic chirp parameter. The double-pulse envelope shapes are modeled by a one-parameter expression of Eq. (12).

lopsided shape of the pulse: when $a < 0.5$, the envelope maximum is shifted toward the earlier time; when $a > 0.5$, it is shifted toward the later time. The effect of a thus skewed pulse shape on the outcome ratio of excited-to-ionized atoms is presented in Fig. 3, where dependencies of the ratio on the value of the parameter a are shown for $\tau = 12$ [which corresponds to the pulse full width at half maximum (FWHM) duration of 42 fs] and for several values of the nominal pulse intensity. As seen, all of the curves demonstrate a monotonic decrease in the ratio value as the parameter a increases, and this trend accelerates when a is close to zero and to unity. Thus, the pulses with the maximum shifted to earlier time result in a considerably larger proportion of the excited atoms, and this proportion is further increased with the laser intensity.

To explore further the enhanced control possibilities provided by an asymmetric pulse shape, we consider a family of pulse shapes with a two-maxima envelope function. In experimental realization, such double pulses are produced using a π -step spectral phase mask; they are utilized in various applications [31,32]. When combined with the mentioned spectral chirp manipulation to form the spectral shape $E(\omega) \sim \exp[-\omega^2/(2\sigma) + i\alpha\omega^2 + i\beta\omega^3 + i\pi\Theta(\omega)]$, this produces a

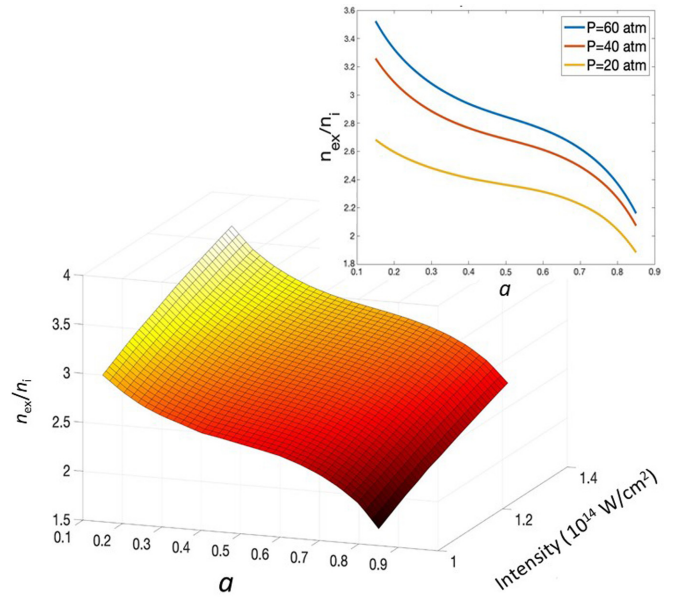


FIG. 3. The effect of the laser pulse asymmetry on the concentration ratio of excited and ionized atoms in dense argon gas (at 60 atm pressure) in the immediate pulse wake. The ratio is plotted as a function of the asymmetry parameter a defined in Eq. (10). The nominal pulse intensity values correspond to $a = 0.5$, with the laser pulse FWHM duration of 42 fs. Inset: modification of a central slice of the surface (nominal intensity of 1.28×10^{14} W/cm²) with the gas pressure.

double-pulse envelope with controllable amplitudes of the subpulses, as represented in Fig. 2(b). In this case, effective strong-field ionization can take place around either one or two maxima or around each of them. In this situation, the envelope normalization by the pulse fluence becomes insufficient for our purposes of exploring the control options, because the second subpulse brings about a trivial overall increase in both the electron density and the excited-atom density. To abstract from this effect, we normalize the laser pulse envelope by the cumulative degree of the initial strong-field (ADK) ionization.

For numerical convenience, we model the double-pulse envelopes with the one-parameter envelope functions,

$$s_{b,\tau}(t) = \frac{c(b)}{1 + |b|} \sqrt{\frac{8\tau_0}{3\tau}} \left\{ 1 + b \tanh \left[\beta \left(\frac{t}{\tau} - \frac{1}{2} \right) \right] \right\} \times \cos^2 \left[\pi \left(\frac{2t}{\tau} - \frac{1}{2} \right) \right] \Theta(t) \Theta(\tau - t), \quad (12)$$

where the control parameter b varies in the interval $(-1, 1)$ and determines the relative amplitudes of the two subpulses: at $b = 0$, the subpulses are of equal amplitude, at $b = 1$, the first subpulse is completely suppressed, and at $b = -1$, the second subpulse is suppressed. The total duration of the double pulse is τ , and the normalization factor $c(b)$ is calculated for each value of b by computing the integrated ionization output according to the ADK expression. The model double pulse is modulated by a soft-step function with the width parameter $\beta = 30$.

One may expect the parameter b to work as an effective control parameter when its absolute value is kept relatively

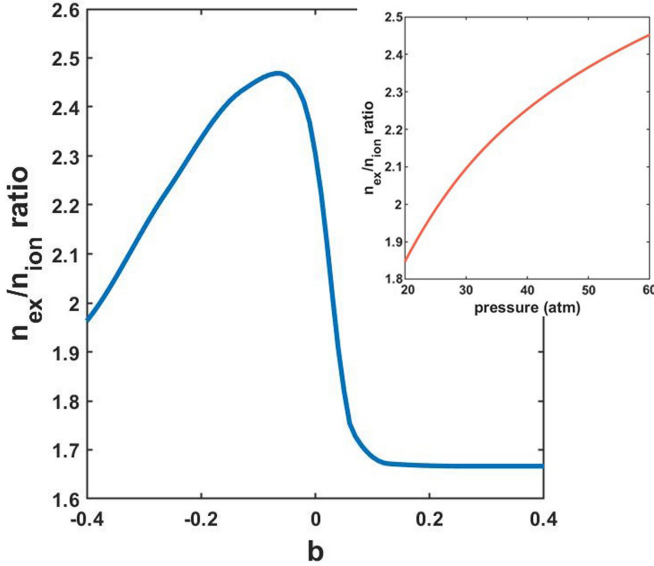


FIG. 4. The ratio of densities of excited and ionized atoms at the end of the laser pulse as a function of the pulse-shape parameter b , as determined in Eq. (12). Inset: the dependence of the ratio's peak value on the gas pressure.

small, that is, when the two subpulses have comparable magnitudes. In this regard, it is instructive to compare the buildup dynamics of the ionic and excited-atom densities in the two cases, in which the pulse-shape parameter b has positive and negative signs while having the same small absolute value. For the positive b , the weaker first subpulse is followed by the stronger second subpulse; as a result, the dynamics of excitation and ionization keeps a low profile during and after the first subpulse, so that the contributions to the final values of n_{ex} and n_{ion} are almost entirely determined by the second subpulse. In contrast, for the negative b , the stronger first subpulse is followed by the weaker second subpulse; in this case, the first subpulse produces a considerable number of free electrons to be actively engaged in the impact processes right at the start of the second subpulse.

The outcome control pattern is presented in Fig. 4, which shows the ratio of $n_{\text{ex}}/n_{\text{ion}}$ as a function of b . The curve presented in Fig. 4 has two salient features. First, it indicates that the effective control is achieved in a rather narrow region of small values of $|b|$. The physical reason for this is the mentioned strong nonlinearity of the processes involved. Indeed, the control is effected by the interplay of the collisional processes, and for this interplay, one needs to have enough free electrons in the first place. This is why no control is expected in the case when the strong subpulse comes second. In this case, the electrons are mostly released by the second subpulse, and thus they are not affected by the first subpulse. On the other hand, if the first subpulse is strong but the second subpulse is very weak, the electrons are produced in multitude, but the second subpulse does not impart sufficient energy in these electrons to cause an outcome different from that generated by the first subpulse acting alone.

The second salient feature is that the curve is decidedly lopsided, peaking at negative values of b and having a broader left shoulder. This asymmetry can be explained by the same

notion of the additional supply of free electrons and their engagement in the collisional processes. The negative values of b correspond to the situation when the stronger subpulse comes first, with the consequence of the aforementioned head start of the n_{ex} and n_{ion} dynamic multiplication.

When the $n_{\text{ex}}/n_{\text{ion}}$ ratio is considered as a function of the laser intensity as a fixed value of $b = -0.06$ (which corresponds to the maximum of the curve in the lower panel in Fig. 3), it demonstrates steady growth with increasing intensity and can be conveniently fitted by a fifth-order polynomial of the dimensionless variable $x = U_p/U_{p0}$, being the ratio of the ponderomotive energy U_p to the standard value of $U_{p0} = 7$ eV at the laser intensity of 10^{14} W/cm²: in the $0.5 \leq x \leq 1.5$ range, $\ln(n_{\text{ex}}/n_{\text{ion}}) = 17.35 x^5 - 94.30 x^4 + 201.2 x^3 - 210.4 x^2 + 108.0 x - 21.01$, with $R^2 = 0.9996$. This growth agrees well with the underlying notion of the control being enabled and fostered by a sufficient number of free electrons released early in the laser pulse.

The considered double-pulse composite structure allows for sensitive and efficient control of the resulting plasma composition. Overall, one may generalize that pulse-shape modifications shifting the envelope maximum within the pulse will be effective at controlling the density ratio of excited and ionized atoms. It also can be noted that the pulse-shape modification due to propagation effects, such as defocusing of the trailing portion of the pulse, work in this very direction and thus can be anticipated to further enhance the control capabilities. On the other hand, the propagation effects, such as self-focusing, self-steepening, and plasma defocusing, do change the temporal shape of the laser pulse along its trajectory in the filamentation region. One can expect that the ratio will be changing along the filament as well. The ionization and excitation of the medium does in turn affect the propagating laser pulse; the ensuing intertwined development is of separate interest but lies well beyond the scope of this paper. To abstract from these complications in a possible experimental setting [6], we assume that the laser beam is tightly focused (e.g., using a focal length of 15–20 cm), so that the sufficiently high laser intensity is only achieved within the short Rayleigh range. Then, the nonlinear effects, ionization, and excitation are confined to this short distance, and the acting laser pulse can be assumed to hold approximately the shape with which it enters this high-intensity region, and which is determined by the conditions of external focusing and linear propagation.

IV. CONCLUSIONS

In a dense-gas situation, when the interatomic distances are comparable to or smaller than the ponderomotive radius, the evolution of transient electronic and optical characteristics of a filament wake channel depends crucially on the plasma composition at the end of the laser pulse, in terms of the concentrations of the ionized and excited atoms. During the laser pulse, ionization and excitation dynamics are driven by the competition of strong-field ionization and collisional processes. Inverse Bremsstrahlung on neutral atoms provides the released electrons with considerable energy to be spent on collisional excitation and impact ionization. Considering a high-pressure argon gas and using a kinetic model of these

processes, we explored the sensitivity of the composition of highly nonequilibrium plasma, which is formed by the end of the pulse, to the pulse envelope shape. By examining three families of normalized envelopes, we have shown that using asymmetric pulse envelopes skewed toward the earlier time, one can effectively control the ratio of the resulting number densities of excited atoms and ionized atoms. This density ratio control engenders effective control of the electronic

and gas-dynamic processes comprising the wake channel evolution.

ACKNOWLEDGMENTS

This work was supported by the National Science Foundation under Grant No. PHY1806594 and by the Office of Naval Research under Award No. N00014-15-1-2574.

- [1] L. Berge, S. Skupin, R. Nuter, J. Kasparian, and J. P. Wolf, Ultrashort filaments of light in weakly ionized, optically transparent media, *Rep. Prog. Phys.* **70**, 1633 (2007).
- [2] A. Couairon and A. Mysyrowicz, Femtosecond filamentation in transparent media, *Phys. Rep.* **441**, 47 (2007).
- [3] S. L. Chin, *Femtosecond Laser Filamentation* (Springer, New York, 2010), Vol. 55.
- [4] A. Filin, R. Compton, D. A. Romanov, and R. J. Levis, Impact-Ionization Cooling in Laser-Induced Plasma Filaments, *Phys. Rev. Lett.* **102**, 155004 (2009).
- [5] D. A. Romanov, R. Compton, A. Filin, and R. J. Levis, Dynamics of strong-field laser-induced microplasma formation in noble gases, *Phys. Rev. A* **81**, 033403 (2010).
- [6] X. H. Gao, G. Patwardhan, S. Schrauth, D. W. Zhu, T. Popmintchev, H. C. Kapteyn, M. M. Murnane, D. A. Romanov, R. J. Levis, and A. L. Gaeta, Picosecond ionization dynamics in femtosecond filaments at high pressures, *Phys. Rev. A* **95**, 013412 (2017).
- [7] S. Varma, Y. H. Chen, and H. M. Milchberg, Trapping and Destruction of Long-Range High-Intensity Optical Filaments by Molecular Quantum Wakes in Air, *Phys. Rev. Lett.* **101**, 205001 (2008).
- [8] J. H. Odhner, D. A. Romanov, and R. J. Levis, Rovibrational Wave-Packet Dispersion During Femtosecond Laser Filamentation in Air, *Phys. Rev. Lett.* **103**, 075005 (2009).
- [9] S. Zahedpour, J. K. Wahlstrand, and H. M. Milchberg, Quantum Control of Molecular Gas Hydrodynamics, *Phys. Rev. Lett.* **112**, 143601 (2014).
- [10] N. Jhajj, Y. H. Cheng, J. K. Wahlstrand, and H. M. Milchberg, Optical beam dynamics in a gas repetitively heated by femtosecond filaments, *Opt. Express* **21**, 28980 (2013).
- [11] G. Point, C. Milian, A. Couairon, A. Mysyrowicz, and A. Houard, Generation of long-lived underdense channels using femtosecond filamentation in air, *J. Phys. B: At. Mol. Opt. Phys.* **48**, 094009 (2015).
- [12] V. V. Bukin, S. V. Garnov, A. A. Malyutin, and V. V. Strelkov, Interferometric diagnostics of femtosecond laser microplasma in gases, *Phys. Wave Phenom.* **20**, 91 (2012).
- [13] Y. H. Chen, S. Varma, T. M. Antonsen, and H. M. Milchberg, Direct Measurement of the Electron Density of Extended Femtosecond Laser Pulse-Induced Filaments, *Phys. Rev. Lett.* **105**, 215005 (2010).
- [14] D. Romanov, A. Filin, R. Compton, and R. Levis, Phase matching in femtosecond BOXCARS, *Opt. Lett.* **32**, 3161 (2007).
- [15] R. Compton, A. Filin, D. A. Romanov, and R. J. Levis, Observation of Broadband Time-Dependent Rabi Shifting in Microplasmas, *Phys. Rev. Lett.* **103**, 205001 (2009).
- [16] R. Compton, A. Filin, D. A. Romanov, and R. J. Levis, Dynamic Rabi sidebands in laser-generated microplasmas: Tunability and control, *Phys. Rev. A* **83**, 053423 (2011).
- [17] D. A. Romanov and R. J. Levis, Evolution of laser microfilaments in the wake of a femtosecond driving pulse, *Phys. Rev. A* **87**, 063410 (2013).
- [18] S.-F. Zhao, L. Anh-Thu, C. Jin, X. Wang, and C. D. Lin, Analytical model for calibrating laser intensity in strong-field-ionization experiments, *Phys. Rev. A* **93**, 023413 (2016).
- [19] H. Zimmermann, S. Patchkovskii, M. Ivanov, and U. Eichmann, Unified Time and Frequency Picture of Ultrafast Atomic Excitation in Strong Laser Fields, *Phys. Rev. Lett.* **118**, 013003 (2017).
- [20] D. A. Romanov and R. J. Levis, Delayed ionization and excitation dynamics in a filament wake channel in a dense-gas medium, *Phys. Rev. A* **102**, 013110 (2020).
- [21] D. A. Romanov, X. H. Gao, A. L. Gaeta, and R. J. Levis, Intrapulse impact processes in dense-gas femtosecond laser filamentation, *Phys. Rev. A* **97**, 063411 (2018).
- [22] M. V. Ammosov, N. B. Delone, and V. P. Krainov, Tunnel ionization of complex atoms and atomic ions in alternating electromagnetic field, *Sov. Phys. JETP* **64**, 1191 (1986).
- [23] E. Gargioni and B. Grosswendt, Electron scattering from argon: Data evaluation and consistency, *Rev. Mod. Phys.* **80**, 451 (2008).
- [24] Y. P. Raizer, *Laser-Induced Discharge Phenomena* (Consultants Bureau, New York, 1977).
- [25] W. Lotz, An Empirical Formula for Electron-Impact Ionization Cross-Section, *Z. Angew. Phys.* **206**, 205 (1967).
- [26] L. R. Peterson and J. E. Allen, Electron-Impact Cross-Sections for Argon, *J. Chem. Phys.* **56**, 6068 (1972).
- [27] R. Trebino, *Frequency-Resolved Optical Gating: The Measurement of Ultrashort Laser Pulses* (Kluwer Academic, New York, 2000).
- [28] B. Khubchandani, A. C. Silva, P. N. Guzdar, and R. Roy, Using GRENOUILLE to characterize asymmetric femtosecond pulses undergoing self- and cross-phase modulation in a polarization-maintaining optical fiber, *Opt. Express* **11**, 3063 (2003).
- [29] C. Rullière, *Femtosecond Laser Pulses: Principles and Experiments* (Springer, New York, 2005).
- [30] A. Efimov, C. Schaffer, and D. H. Reitze, Programmable Shaping of Ultrabroad-Bandwidth Pulses from a Ti-Sapphire Laser, *J. Opt. Soc. Am. B: Opt. Phys.* **12**, 1968 (1995).
- [31] D. Meshulach and Y. Silberberg, Coherent quantum control of multiphoton transitions by shaped ultrashort optical pulses, *Phys. Rev. A* **60**, 1287 (1999).
- [32] A. Konar, V. V. Lozovoy, and M. Dantus, Stimulated Emission Enhancement Using Shaped Pulses, *J. Phys. Chem. A* **120**, 2002 (2016).